Diamondoid coating enables disruptive approach for chemical and magnetic imaging with 10 nm spatial resolution

Hitoshi Ishiwata,[1,2] Yves Acremann,[3] Andreas Scholl,[4] Eli Rotenberg,[4] Olav Hellwig,[5] Elizabeth Dobisz,[5] Andrew Doran,[4] Boryslav A. Tkachenko,[6] Andrey A. Fokin,[6] Peter R. Schreiner,[6] Jeremy E. P. Dahl,[1] Robert M. K. Carlson,[1] Nick Melosh,[1,7] Zhi-Xun Shen,[1,8,a)] and Hendrik Ohldag[9,b)]

[1]*Stanford Institute for Materials and Energy Science, Stanford University, Stanford, California 94305, USA*
[2]*Department of Electrical Engineering, Stanford University, Stanford, California 94305, USA*
[3]*Swiss Federal Institute of Technology Zurich, Laboratory for Solid State Physics, 8093 Zürich, Switzerland*
[4]*Lawrence Berkeley National Laboratory, Advanced Light Source, Berkeley, California 94705, USA*
[5]*San Jose Research Center, Hitachi Global Storage Technologies, San Jose, California 95135, USA*
[6]*Justus-Liebig University, Institute of Organic Chemistry, Heinrich-Buff-Ring 58, D-35293 Giessen, Germany*
[7]*Department of Material Science and Engineering, Stanford University, Stanford, California 94305, USA*
[8]*Department of Physics and Applied Physics, Stanford University, Stanford, California 94305, USA*
[9]*SLAC National Accelerator Laboratory, Stanford Synchrotron Radiation Laboratory, Menlo Park, California 94025, USA*

(Received 5 July 2012; accepted 17 September 2012; published online 15 October 2012)

Diamondoids are unique molecular nano-materials with diamond structure and fascinating properties such as negative electron affinity and short electron mean free paths. A thin layer of diamondoids deposited on a cathode is able to act as an electron monochromator, reducing the energy spread of photo-emitted electrons from a surface. This property can be applied effectively to improve the spatial resolution in x-ray photoemission electron microscopy (X-PEEM), which is limited by chromatic aberration of the electron optics. In this paper, we present X-PEEM measurements reaching the technological relevant spatial resolution of 10 nm without the need of expensive and complex corrective optics. Our results provide a simple approach to image surface chemical and magnetic information at nanometer scales by employing diamondoids. © *2012 American Institute of Physics*. [http://dx.doi.org/10.1063/1.4756893]

Diamond is a wide band gap insulator that combines material properties such as high refractive index, mechanical hardness, high thermal conductance, negative electron affinity (NEA), and biocompatibility, making it attractive for applications like photon management,[1] mechanical coatings,[2] heat management for semiconductor chips,[3] electron emitters,[4] and drug delivery.[5,6] Recently, applications for nanometer scale diamond particles (5–50 nm), often referred to as nano-diamonds, have developed rapidly, ranging from bio-medical[5] to quantum computing.[7] Even smaller, molecular-scale diamonds are known as "diamondoids," consisting of only a few diamond unit cells.[8] Measurements of tetramantane thiol monolayers on Au and Ag surfaces recently revealed that these molecules are also NEA materials,[9] where the vacuum level lies below the lowest unoccupied molecular orbital (LUMO). This property combined with strong electron phonon scattering and extremely short mean free path in diamondoid caused monochromatization of secondary electrons emitted from a metal surface.[10] The electron emission spectrum is characterized by a sharp peak with a bandwidth of 0.3 eV (FWHM), which surpasses the value that is obtained on bulk diamond.[9,10] Hence, diamondoids offer the promise of a disruptive approach to design photo-cathodes with superior emission properties. However, applications which are based on the ability to effectively transform electron energy with as little as a single layer of diamondoids have not yet been demonstrated.

In x-ray photoemission electron microscopy (X-PEEM), a sample is illuminated using polarized and monochromatic x-rays typically generated by a synchrotron. The absorption of x-rays leads to emission of photo- and secondary electrons from the sample surface acting as a cathode. Because of its element, chemical, and spin structure specificity, it is used by researchers from a variety of disciplines for composition mapping and analysis.[11–14] The spatial resolution in X-PEEM is limited by the spherical and chromatic abberation coefficients of the electrostatic lens system to typically about 25 nm.[15–18] Because the photoexcited primary and secondary electrons exhibit a broad energy distribution, the effect of chromatic aberration on the formation of the image is significant in the case of X-PEEM. If ultraviolet excitation is used, the energy spread can be reduced to 1 eV or less and 10 nm spatial resolution are observed;[15] however, the improved spatial resolution comes at the cost of elemental, chemical, and magnetic sensitivities. Another approach is to introduce corrective electron optics into the microscope.[15–18] However, this comes at significant costs (>$1M) compared to conventional PEEM (~$100k) and makes the operation much more complex. In this paper, we show how the effect of chromatic aberrations in X-PEEM can be minimized without compromising the functionality or the setup of the instrument at minimal cost using a thin diamondoid coating, by a layer of [121] tetramantane-thiol,[9,10] which forms a self-assembled monolayer (SAM) on selected metal surfaces.[19–24] Our findings represent the application of diamondoids to effectively improve the performance of an electron cathode.

a)email: zxshen@stanford.edu.
b)email: hohldag@slac.stanford.edu.

To illustrate the idea behind our approach, we will briefly describe the effects of the diamondoid coating on the energy distribution of the electrons emitted from the surface in an x-ray absorption spectroscopy setup as it is shown in Figure 1. Soft x-rays with photon energies of several hundred electron volts impinge on the surface. At certain photon energies characteristic for the elements present in the sample, the absorption of soft x-rays will occur through the resonant excitation of core level electrons into empty valence states (1). Subsequent recombination of the excited state causes the emission of an Auger electron (2). Both the Auger and the photoelectron will travel to the surface, lose their energy through inelastic scattering, and generate a cascade of secondary electrons (3) with a wide energy distribution (>5 eV) as shown by the black curve in Figure 1 (taken from Ref. 25). Without the diamondoid coatings, these secondary electrons are directly emitted into the vacuum and contribute to the image formation in X-PEEM. To limit the effects of chromatic aberration of the lens system, an aperture is typically mounted in the back focal plane of the objective lens that rejects 90% or more of the electrons but at the same time reduces the effect of chromatic aberrations.[16,17] Using apertures with a diameter of 10–20 μm, one can achieve a spatial resolution of about 25 nm,[15,18] while still maintaining practical image intensity. Upon coating the sample surface with a monolayer of diamondoids, the energy distribution of the emitted electrons, however, changes dramatically. The negative electron affinity and efficient electron scattering process cause the electrons passing through the diamondoid surface layer to be scattered and to relax to the LUMO (4) before they are emitted into the vacuum.[9,10] Consequently, their energy distribution is much smaller as shown by the red curve in Figure 1, which has been acquired using x-rays with a photon energy of 700 eV from a diamondoid coated Au surface using a Scienta hemispherical analyzer. To benchmark, we also compare this data with earlier data acquired at 55 eV (Ref. 9) (green), as well as data obtained using a UV source without diamondoid coating.[25] (blue line). Sample current for all measurements is between 2 and 10 nA. The electron energy mono-chromatization effect still functions as effectively at 700 eV, which is an order of magnitude higher than earlier experiments using 55 eV photons.[9] In summary, we find similar energy spreads after excitation with 700 eV x-ray photons on a diamondoid covered surface as after excitation with 5 eV UV photons from a bare surface.

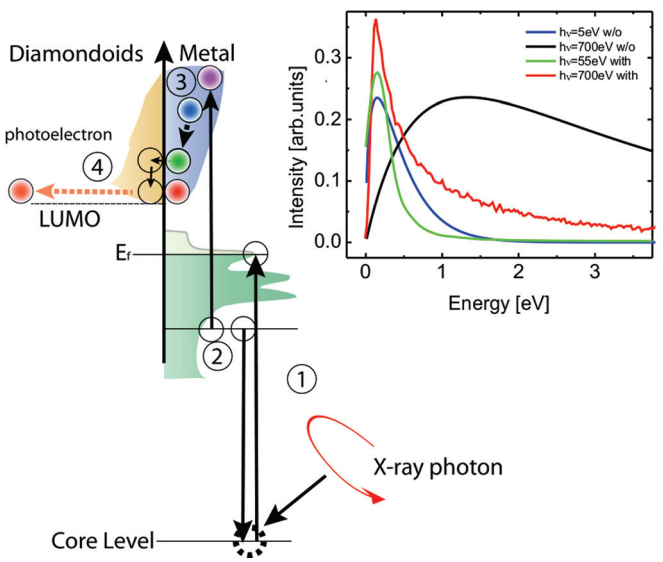

FIG. 1. Effect of the diamondoid coating on energy distribution of the secondary electron yield following x-ray absorption. (1) Resonant absorption of a soft x-ray photon by excitation of a core level electron into an empty valence state. (2) Recombination of excited state through emission of an Auger electron. (3) Generation of secondary electrons through inelastic scattering of Auger electron and photo electron. (4) Mono-chromatization of secondary electrons in diamondoid layer followed by emission from LUMO. Inset shows energy distribution of secondary electrons ejected from a metal (Au) surface after excitation by 700 eV x-ray photons with (red) and without (black) the diamondoid coating. Also shown, the energy distribution of secondary electrons after excitation by 5 eV UV-photons (blue) without diamondoid coating and 55 eV extreme UV photons (green) with diamondoid coating.

For our experiments, we used the state of art PEEM3 microscope[18] installed at the Advanced Light Source, a soft x-ray synchrotron in Berkeley, CA (USA).[26] Images with magnetic contrast were obtained using x-ray magnetic circular dichroism (XMCD).[27] For this purpose, the energy of the incoming x-rays is tuned to the L absorption resonance where the XMCD effect is most pronounced and two images are acquired with opposite circular polarization of the incident x-rays and subtracted from each other. In our case, we tuned the energy to the Co L_3 resonance at 778.1 eV since all our magnetic samples are based on cobalt. The resulting images do not contain topographic or chemical but only magnetic information.[11] An image consisting of only topographic and work function contrast can be obtained in a similar manner by computing the sum of the two images. Images with chemical contrast as shown later were acquired by subtracting images taken on and off resonance, in this case the carbon π^* resonance at 284.7 eV with linear polarization. No additional image processing has been applied.[18]

For our experiments, we obtained X-PEEM images from different samples which exhibit magnetic, topographic, and chemical contrasts. Co/Pd multilayer samples were prepared using sputter deposition at Hitachi Global Storage Technologies.[28] The layer structure of the magnetic material was ([Co(0.5 nm)Pd(0.7 nm)] × 40), producing magnetic films that will align the magnetization perpendicular to the sample surface. The same layered structure was used for the bit-patterned media (BPM) sample. To obtain a BPM sample, however, 35 nm sized Si islands separated by 25 nm grooves, which are also 25 nm deep, were prepared using a lithographic process.[25,29] The magnetic material was then deposited on top.

We present results obtained on larger structures (~120 nm). For this purpose, we acquired images of magnetic domains in a continuous Co/Pd multilayer sample. The magnetization in adjacent domains points either out of or into the sample surface creating a domain pattern that can be observed using the XMCD effect. The domain size distribution is very homogeneous in these samples over large areas,[28] which is why they are often used as a standard for magnetic imaging.[30] We systematically decreased the spatial resolution of the microscope by reducing the acceleration voltage and increasing the size of the back focal aperture from its optimal condition.[29] By reducing the acceleration voltage, the effect of chromatic aberration—which is proportional to ΔE/E—is increased, and by opening the back focal aperture, a larger bandwidth is accepted into the microscope, also increasing the

effect of chromatic aberration on the image. For example, using a low acceleration voltage of 10 kV (5 kV/mm), as shown in Figure 2(a), the magnetic contrast is barely visible, while the diamondoid coating leads to a significant recovery of the image contrast, so that the main characteristics of the domain pattern can still be observed. The quantitative differences between the two cases (small/large back focal aperture) depending on the acceleration voltage are shown in Figures 2(b) and 2(c). We find that the count rate per image pixel increases in the diamondoid coated samples, although the integrated incoming photon flux measured by a Au grid in front of the microscope was identical for all measurements. This observation is a direct consequence of the 0.6 eV reduction in work function caused by the [121] tetramantane-6-thiol monolayer[31] as well as the increased transfer through the back focal aperture due to the reduced energy spread of the electron yield. In addition, we observe that the image contrast between the white and dark areas is consistently increased by diamondoid coating using identical exposure times as demonstrated in Figure 2(c). Again, this effect is clearly visible in the images as shown in Figure 2(a). At these operating conditions, i.e., low photon flux and low acceleration voltage, the diamondoid coating allows us to resolve magnetic domains that are 120 nm in size, which is not possible when using uncoated samples. These are the very conditions necessary for the analysis of polymers and biological samples that are sensitive to x-ray beam damage. Some of these samples will often degrade within a minute of exposure to x-ray and the ability to increase the observable contrast that can be obtained in short times is crucial to such studies.[32]

We now determine the intrinsic resolution limit of the microscope and show the effect of the diamondoids under these conditions. We obtained images of the magnetic domain pattern as well as the topography of so called magnetic

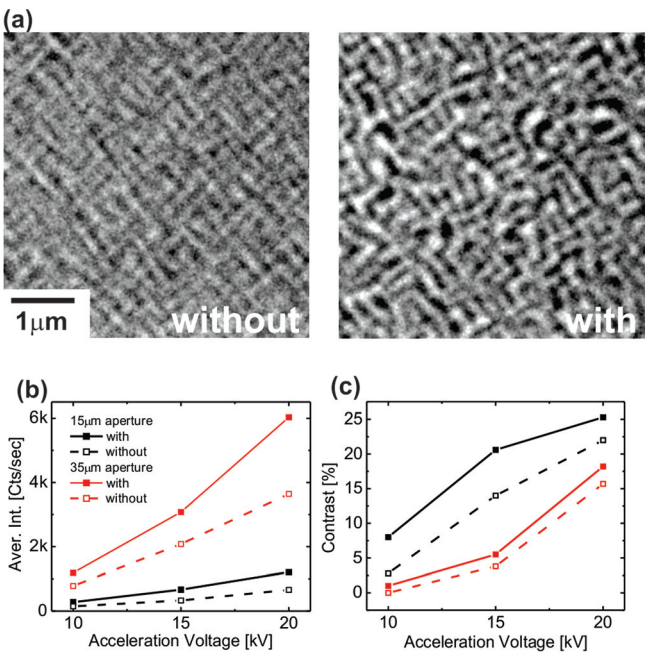

FIG. 2. X-PEEM images of magnetic domains in a Co/Pd multilayer obtained at an acceleration voltage of 10 kV and using a back focal aperture of 35 μm. The image on the left hand side was obtained without the diamondoid coating and the image on the right hand side with the diamondoid coating. In both cases, an exposure time of 80 s was chosen.

BPM. We acquired images with the diamondoid SAM on top of the sample, and then evaporated the diamondoid layer by annealing at 200 °C for 10 min allowing us to take an image of the same spot with and without the diamondoid coating. Using magnetic XMCD contrast, we show in the top row of Figure 3 that our before and after images were indeed taken from the same spot on the sample. Since the maximum contrast that can be obtained using the XMCD effect is of the order of 10%, we already observe an improvement of the image contrast for the 60 nm BPM sample. The beneficial effect of the diamondoid coating can be recognized in these images, e.g., in the area marked with a red rectangle exhibiting a checkerboard domain pattern.

The effect becomes much clearer when the topography images are analyzed. The topography image on the right of Figure 3(a) shows uninterrupted vertical and horizontal lines that represent 25 nm grooves as well as 35 nm islands. These grooves can hardly be resolved by eye in the image on the left, obtained without diamondoids, indicating that the spatial resolution of the microscope is indeed approximately 25 nm and also that the diamondoid coating improves the spatial resolution beyond this point. Note that in both cases the topography images show additional contrast on a scale of several micrometers. This contrast most likely originates from residual photochemicals from the lift-off process that causes variations in work function as well as the chemical state of Co in the topmost layers. Altogether, the images with magnetic and topographic contrast as well as the line scans clearly show that the diamondoid coating is able to improve the spatial resolution of X-PEEM well beyond its current limits of 25 nm.

The final step is to show that a spatial resolution of 10 nm with chemical contrast can be achieved using diamondoid coating in X-PEEM. A sample consisting of Au nanoparticles was prepared by depositing poly-L-lysine (PLL) on top of silicon. Au nanoparticles of sizes 10 nm $\pm$ 3 nm were then deposited on top of PLL and coated with 3 nm Ti and 3 nm Ag. All of the nanoparticles were coated with diamondoids using a method described in Refs. 20 and 21 that has been shown to be able to reliably obtain monolayer coating on metal surfaces.[33] Due to a thin layer of Ag, diamondoid nanowires were formed on top of the nanoparticle sample at sizes ranging from 20 nm to 100 nm,[34] as detected by scanning electron microscopy (not shown). Such a sample was chosen, because it provides topographic as well as chemical contrast over a wide range of length scales from a few nm to hundreds of nm. Chemical contrast is observed because this hybrid organic-inorganic material incorporates organic linkers (diamondoids) together with inorganic clusters to form crystalline materials such as nanoribbons, nanowires, and lamellar sheets.[35] Nanoparticle and nanowires incorporate sp^2 carbon, which exhibits a strong resonance in soft x-ray absorption at 284.5 eV, the so called C-π^* resonance. To obtain an image of the spatial distribution of the carbon sp^2 density, one needs to acquire an image at the carbon π^* resonance and normalize this to an image obtained off-resonance at 280 eV. Figure 4(a) shows the result in which one can clearly recognize that the density of carbon π^* orbitals is increased on the nanostructures (Figure 4(a)). This observation is further corroborated by acquiring

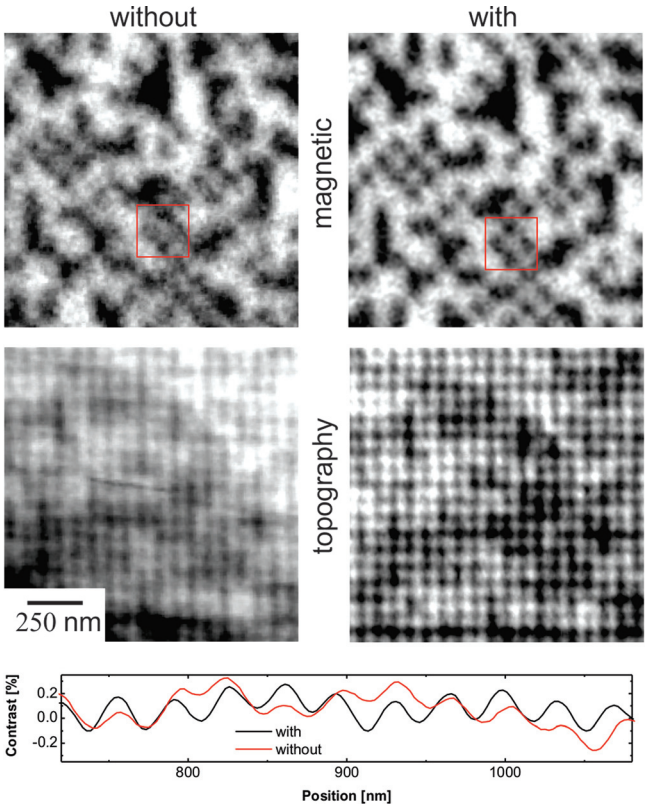

FIG. 3. X-PEEM images of magnetic domains (top row) and the topography (bottom row) of Co/Pd bit patterned media with a period of 60 nm/(35 nm bits/25 nm spacing). The total exposure time was 300 s. The left column shows images without the diamondoid coating and the right column images obtained with diamondoid coating. Magnetic and topographic images were obtained at the same area of the sample. The bottom panel shows horizontal line scans of the sample with (black) and without (red) diamondoid coating to illustrate the resolution improvement.

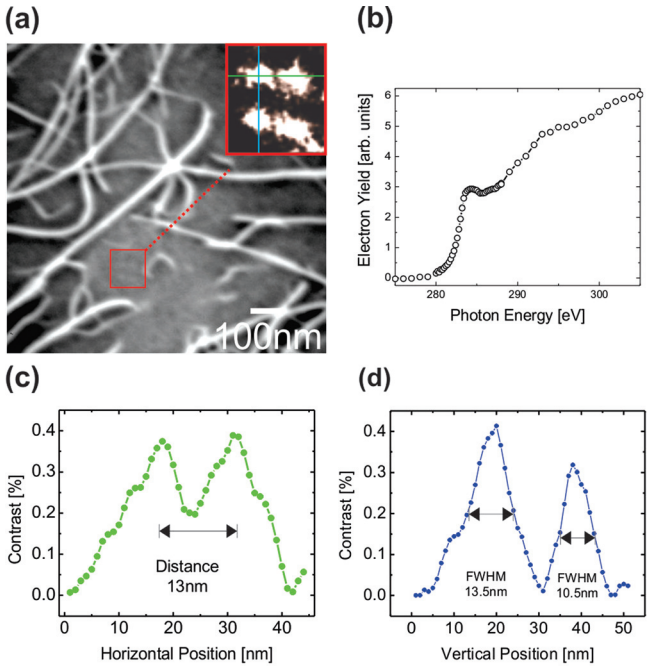

FIG. 4. (a) X-PEEM image of the same sample obtained using chemical contrast mechanism at the carbon π^* resonance. The nanowires as well as the nanoparticles (see inset) can clearly be identified and resolved. An exposure time of 120 s was used. (b) XAS spectrum obtained from the nanowires, which appear white in (a). The peak at 284.7 eV is indication of the presence of π^*-orbitals, indicative of sp^2 bonding. The image was obtained using this photon energy. (c) Horizontal linescan across the inset in (a). The spacing between the particles is 13 nm. (d) Vertical linescan across the inset in (a). The size of the particles is determined to be 10.5 nm and 13.5 nm.

local x-ray absorption spectra on the nanoparticles and normalizing them to absorption spectra acquired on the background. For this purpose, a series of XPEEM images were acquired at discrete energies between 275 eV and 310 eV and the image intensity integrated over the area of several nanowires was normalized to a similar area on the Si wafer nearby. Such a spectrum is shown in Figure 4(b). It exhibits a distinct peak at 284.5 eV, which is indicative of the presence of π^* orbitals, in combination with the existence of a sp^2 bonding situation. Hence, the contrast shown in Figure 4(a) is of true chemical origin. A magnified image of a small area, as indicated by the red box in Figure 4(b), is shown in Figure 4(c) revealing four round objects 10–13 nm in size. These objects represent the original Au nanoparticles that were deposited on the surface. Horizontal and vertical linescans (Figure 4(d)) confirm their size and spacing to be ranging from 10 to 13 nm. Again the origin of the contrast is the increased density of sp^2 hybridized carbon. Changes of the chemical coordination of carbon can be observed on a length scale of 10 nm. We can therefore conclude that we were able to obtain images with chemical contrast and 10 nm spatial resolution in X-PEEM.

The spatial resolution of a microscope can be uniquely quantified measuring its transfer function, i.e., the evolution of contrast for different sized objects. We therefore determined the contrast transfer in our X-PEEM from different samples as discussed before using identical imaging conditions (20 kV acceleration voltage/10 μm aperture). For this purpose, we calculated the image contrast of different objects with different lateral size and normalized this value to the contrast observed for much larger structures with identical origin, like larger magnetic domains away from the patterned area or "large bundles" of nanowires. The transfer functions obtained for samples with and without diamondoid coating are shown on a so called Bode (magnitude) plot in Figure 5, where the amplitude of the contrast transfer is plotted versus the spatial frequency, that is $1/(2d)$. The typical behavior of the transfer function, when plotted this way, is that it is constant, or only slowly decreases up to a certain frequency and then drops off linearly until it reaches zero. The length scale for which the contrast can still be detected is identified as the spatial resolution of the optical system. The observation is that the contrast transfer is practically unaffected until a spatial frequency of 5 μm^{-1} (100 nm objects) in the coated samples, while the contrast in images without coating already shows a significant decrease of about 50% at this length scale. Without the diamondoid coating, the contrast transfer (red) decays quickly and reaches 3% at 25 nm. On the other hand, the coated samples consistently show a contrast increase by a factor of ~2.5. In summary, we find that at 25 nm the contrast transfer is still significant on samples with the diamondoid coating reaching its limit at 10 nm.

In summary, we find that diamondoid SAMs coatings: (1) increase the transfer function of the microscope on average by a factor of 2.2–2.5, (2) allowing us to obtain images with improved contrast of samples that are sensitive to x-rays or

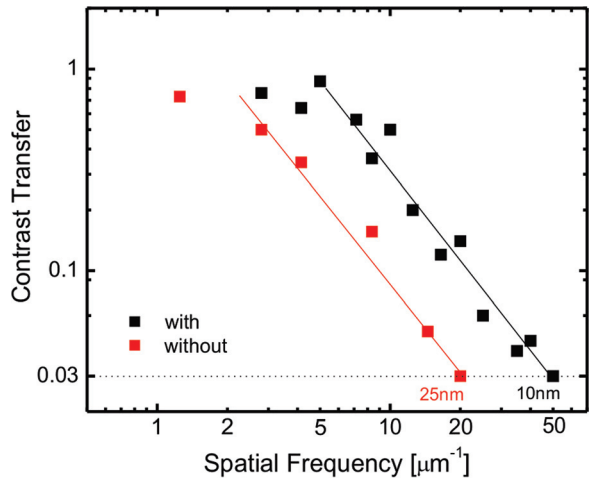

FIG. 5. Optical transfer function determined using coated (black) and uncoated (red) samples. In all cases, the acceleration voltage has been set to 20 kV and the 15 μm aperture has been used. Data have been obtained using magnetic, topographic, and chemical contrasts using the samples discussed in Figures 2–4, The diamondoid coating leads to a consistent increase in contrast transfer of 2.5. Maximum contrast is obtained up to structure sizes of 100 nm (5 μm^{-1}), while the contrast transfer of uncoated samples is already reduced by a factor of two. Ultimately 10 nm structures can be resolved (3% contrast transfer) using diamondoid coating.

electric fields without sacrificing resolution, (3) improve the ultimate spatial resolution to 10 nm and reduce exposure times overall, which are particularly relevant for time-resolved microscopy studies and studies where small contrasts originating from interfaces or small variations in chemistry across surfaces are of interest. In this study, we focused on metal surfaces covered with diamondoids via a thiol bond. However, results indicate that similar stable bindings can be achieved on oxide surfaces[36,37] or directly on Si surfaces[38] without the need to deposit a metallic sticking layer first. This will extend the application of this simple and inexpensive "X-PEEM resolution booster" to many more systems of interest.

The work at the Stanford Institute for Materials and Energy Sciences was supported by the DOE Office of Basic Energy Sciences, Division of Materials Sciences. SSRL/SLAC is a user facility within the Office of Science operated for the U.S. Department of Energy Office of Science by Stanford University, The Advanced Light Source is supported by the Director, Office of Science, Office of Basic Energy Sciences, of the U.S. Department of Energy under Contract No. DE-AC02-05CH11231. The work in Giessen (Germany) was also supported by a grant through the German Research Foundation coupled with the National Science Foundation of the USA (DFG-NSF).

[1]T. Schroder, A. W. Schell, G. Kewes, T. Aichele, and O. Benson, Nano. Lett. **11**, 198–202 (2011).
[2]M. D. Drory and J. W. Hutchinson, Science **263**, 1753–1755 (1994).
[3]W. Lanhua, P. K. Kuo, R. L. Thomas, T. R. Anthony, and W. F. Banholzer, Phys. Rev. Lett. **70**, 3764–3767 (1993).
[4]J. R. Smith, G. L. Bilbro, and R. J. Nemanich, Phys. Rev. B **76**, 245327 (2007).
[5]V. N. Mochalin, O. Shenderova, D. Ho, and Y. Gogotsi, Nature Nanotechnol. **7**, 11–23 (2012).
[6]X. Q. Zhang, R. Lam, X. Xu, E. K. Chow, H. J. Kim, and D. Ho, Adv. Mater. **23**, 4770–4775 (2011).
[7]I. Aharonovich, A. D. Greentree, and S. Prawer, Nature Photon. **5**, 397–405 (2011).
[8]J. E. Dahl, S. G. Liu, and R. M. K. Carlson, Science **299**, 96–99 (2003).
[9]W. L. Yang, J. D. Fabbri, T. M. Willey, J. E. Dahl, R. M. K. Carlson, P. R. Schreiner, M. A. Kelly, Z. Hussain, N. A. Melosh, Z. X. Shen *et al.*, Science **316**, 1460–1462 (2007).
[10]W. A. Clay, Z. Liu, W. Yang, J. D. Fabbri, J. E. Dahl, R. M. K. Carlson, P. R. Schreiner, P. A. Pianetta, N. Melosh, Z. X. Shen *et al.*, Nano Lett. **9**, 57–61 (2009).
[11]H. Ohldag, T. J. Regan, J. Stöhr, A. Scholl, F. Nolting, J. Lüning, C. Stamm, S. Anders, and R. L. White, Phys. Rev. Lett. **87**, 247201 (2001).
[12]Y. Ma, B. Aichmayer, O. Paris, P. Fratzl, A. Meibom, R. A. Metzler, Y. Politi, L. Addadi, P. U. P. A. Gilbert, and S. Weiner, Proc. Natl. Acad. Sci. U.S.A. **106**, 6048–6053 (2009).
[13]B. O. Leung, A. P. Hitchcock, J. L. Brash, A. Scholl, and A. Doran, Adv. Eng. Mater. **12**, B133–B138 (2010).
[14]Q. He, Y. H. Chu, J. T. Heron, S. Y. Yang, W. I. Liang, C. Y. Kuo, H. J. Lin, P. Yu, A. Scholl, R. Ramesh *et al.*, Nat. Commun. **2**, 225 (2011).
[15]E. Bauer, J. Phys. Condens. Matter **21**, 314001 (2009).
[16]R. Wichtendahl, R. Fink, H. Kuhlenbeck, D. Preikszas, H. Rose, R. Spehr, Th. Schmidt, E. Bauer, G. Benner, and E. Umbach, Surf. Rev. Lett. **5**, 1249–1256 (1998).
[17]R. M. Tromp, J. B. Hannon, A. W. Ellis, W. Wan, A. Berghaus, and O. Schaff, Ultramicroscopy **110**, 852–861 (2010).
[18]J. Feng, E. Forest, A. A. MacDowell, M. Marcus, H. Padmore, S. Raoux, D. Robin, A. Scholl, D. H. Wei, Y. Wu *et al.*, J. Phys. Condens. Matter **17**, S1339 (2005).
[19]B. A. Tkachenko, N. A. Fokina, L. V. Chernish, J. E. P. Dahl, Shenggao, R. M. K. Carlson, A. A. Fokin, and P. R. Schreiner, Org. Lett. **8**, 1767–1770 (2006).
[20]C. D. Bain and G. M. Whitesides, Science **240**, 62–63 (1988).
[21]J. C. Love, L. A. Estroff, J. K. Kriebel, R. G. Nuzzo, and G. M. Whitesides, Chem. Rev. **105**, 1103–1169 (2005).
[22]T. M. Willey, J. D. Fabbri, J. R. Lee, P. R. Schreiner, A. A. Fokin, B. A. Tkachenko, N. A. Fokina, J. E. Dahl, T. van Buuren, N. A. Melosh *et al.*, J. Am. Chem. Soc. **130**, 10536–10544 (2008).
[23]T. M. Willey, J. R. I. Lee, J. D. Fabbri, D. Wang, M. H. Nielsen, J. C. Randel, P. R. Schreiner, A. A. Fokin, N. A. Melosh, T. van Buuren *et al.*, J. Electron Spectrosc. Relat. Phenom. **172**, 69–77 (2009).
[24]L. Landt, M. Staiger, D. Wolter, K. Klünder, P. Zimmermann, P. R. Schreiner, B. A. Tkachenko, A. A. Fokin, T. Möller, C. Bostedt *et al.*, J. Chem. Phys. **132**, 024710 (2010).
[25]J. Feng and A. Scholl, *Science of Microscopy* (Springer, New York, 2007), p. 657.
[26]T. Warwick, W. McKinney, E. Domning, A. Doran, and H. Padmore, Synchrotron. Radiat. Instrum. **879**, 469–472 (2007).
[27]S. Anders, H. A. Padmore, R. M. Duarte, T. Renner, T. Stammler, A. Scholl, M. R. Scheinfein, J. Stöhr, L. Séve, and B. Sinkovic, Rev. Sci. Instrum. **70**, 3973–3981 (1999).
[28]O. Hellwig, J. B. Kortright, A. Berger, and E. E. Fullerton, J. Magn. Magn. Mater. **319**, 13 (2007).
[29]O. Hellwig, J. K. Bosworth, E. Dobisz, D. Kercher, T. Hauet, G. Zeltzer, J. D. Risner-Jamtgaard, D. Yaney, and R. Ruiz, Appl. Phys. Lett. **96**, 052511 (2010).
[30]O. Hellwig, G. Denbeau, J. B. Kortright, and E. E. Fullerton, Physica B **336**, 136 (2003).
[31]D. M. Alloway, M. Hofmann, D. L. Smith, N. E. Gruhn, A. L. Graham, R. Colorado, Jr., V. H. Wysocki, T. R. Lee, P. A. Lee, and N. R. Armstrong, J. Phys. Chem. B **107**, 11690–11699 (2003).
[32]F. J. Meyer zu Heringdorf, M. C. Reuter, and R. M. Tromp, Nature **412**, 517–520 (2001).
[33]J. C. Randel, Ph.D. dissertation, Stanford University, Stanford, 2011, pp. 82–87.
[34]W. Bin, N. Melosh, "Predicatable morphologies of self-assembled diamondoid-silver thiol wires and sheets" (unpublished).
[35]A. B. Lysenko, G. A. Senchyk, J. Lincke, D. Lässig, A. A. Fokin, E. D. Butova, P. R. Schreiner, H. Krautscheid, and K. V. Domasevitch, Dalton Trans. **39**, 4223–4231 (2010).
[36]S. R. Wasserman, Y. T. Tao, and G. M. Whitesides, Langmuir **5**, 1074–1087 (1989).
[37]A. Ulman, Adv. Mater. **2**, 573–582 (1990).
[38]S. F. Bent, Surf. Sci. **500**, 879–903 (2002).